JCAMECH

Vol. 50, No. 2, December 2019, pp 375-380
DOI: 10.22059/jcamech.2019.291967.448

Buckling Analysis of a Fiber Reinforced Laminated Composite Plate with Porosity

Yusuf Ziya Yüksel[a,*] *and Şeref Doğuşcan Akbaş*[a]

[a] *Department of Civil Engineering, Faculty of Engineering and Natural Sciences Bursa Technical University, Bursa, Turkey*

ARTICLE INFO

Article history:
Received: 04 November 2019
Accepted: 27 December 2019

Keywords:
Laminated Plate
Porosity
Buckling
First Shear Deformation Plate Theory

ABSTRACT

Fiber-reinforced laminated composites are frequently preferred in many engineering projects. With the development in production technology, the using of the fiber reinforced laminated composites has been increasing in engineering applications. In the production stage of the fiber-reinforced laminated composites, porosities could be occurred due to production or technical errors. After a level of the porosity, the mechanical behaviors of composite materials change significantly. This paper presents buckling analysis of fiber-reinforced laminated composite plate with porosity effects within the first shear deformation plate theory. In the porosity effect, three different porosity models are used in the laminated composite plate. The material properties of the laminas are considered as orthotropic property. In the solution of the problem, the Navier procedure is used for the simply supported plate. Influences of the porosity coefficients, the porosity models, the fiber orientation angles and the sequence of laminas on the critical buckling loads are presented and discussed.

1. Introduction

Fiber reinforced laminated composite materials have been used engineering applications, such as thermal barrier, chemical plant, automotive industries, space shuttle. Because of high strength, fire resistance and lightweight properties. During the production in fiber reinforced laminated composite materials, micro-voids and porosities could occur due to production or technical errors. With porosity, the mechanical behavior of composites changes significantly. So, porosity problems are very important in the mechanical behavior of composites. In the literature, the studies about the mechanical behavior of composite plates with porosity effects are presented briefly as follows; free vibration of a simply supported rectangular functionally graded plate with porosity.

Rezai and Saidi [1] studied free vibration analysis of thick rectangular porous plates. Akbaş [2] analyzed the free vibration and static bending of a simply supported functionally graded plate with the porosity effect. Rezaei et al. [3] examined the free vibration of porous functionally graded rectangular plates by using the first shear deformation plate theory. Wang and Zu [4] investigated the vibration analysis of porous functionally graded plates with temperature-dependent mechanical properties. Askari et al. [5] performed the free vibration analysis of rectangular plate with porous-cellular composed of piezoelectric layers. Ebrahimi et al. [6] investigated the free vibration of the magneto-electro-elastic plate with porosity on elastic foundations. Zhao et al. [7] analyzed the vibration of porous functionally graded plates by using (3-D) elasticity theory. Yang et al. [8] performed free vibration and buckling analyses of porous functionally graded graphene nanocomposite plates by using the Chebyshev-Ritz method. Arshid and Khorshidvand [9] examined free vibration of functionally graded porous circular plate with piezoelectric actuators by using a differential quadrature method. Gao et al. [10] examined nonlinear free vibration of made of graphene platelets with functionally graded nanocomposite plates on elastic foundation. Zhao et al. [11] studied the vibration of functionally graded porous shallow shells by using a unified solution. Demirhan and Taskin [12] examined free vibration and static bending of the functionally graded porous plate by Levy type solution. Kim et al. [13] presented free vibration, bending and buckling analysis of functionally graded microplates with porous by using the classical and first shear deformation plate theory. Heshmati and Jalali [14] investigated the free vibration of circular and annular sandwich plates with radially grade porosity. Xue et al. [15] analyzed free vibration of porous circular, square and rectangular plates based on the isogeometric approach. Zhao et al. [16] performed free vibrations analysis of a porous functionally graded rectangular plate with elastic boundary conditions. Karimiasl et al. [17] studied nonlinear forced vibration of the composite sandwich plate with double curved porous shell. Huang et al. [18] investigated nonlinear forced and free vibrations of the porous functionally graded plate resting nonlinear elastic foundations. Zhou et al. [19] examined the vibration of functionally graded porous plates with temperature-dependent physical properties. Yüksel and Akbaş [20] analyzed the effects of temperature on the vibration responses of laminated plates. Akbaş [21,22,23,24,25] studied the effects of porosities on post-buckling, dynamic and nonlinear behaviors of composite beams. Li et. al. [26] examined dynamic buckling and nonlinear vibration of the porous functionally graded sandwich plate on the Winkler-Pasternak elastic foundation. Nam et. al. [27] investigated buckling and post-buckling behavior of cylindrical functionally

* Corresponding author. Tel.: +90-224-300-3710; e-mail: yusuf.yuksel@btu.edu.tr

graded porous plates under torsion in thermal environment. Chen et. al. [28] examined the bending and buckling behavior of a porous novel functionally graded plate by using the Ritz method. Safaei et.al. [29] analyzed buckling of a laminated porous nanocomposite plate resting on elastic foundation. Jabbari et. al. [30] performed thermal buckling analysis of a circular porous plate with piezoelectric by using first-order shear deformation theory. Cong et. al. [31] presented nonlinear thermomechanical buckling and post-buckling behavior of functionally graded porous plates based on high order shear deformation theory. Dong et. al. [32] investigated buckling behavior of functionally graded nanocomposite cylindrical porous shells. Jabbari et. al. [33] examined buckling of the circular porous plate under uniform radial compression.

The aim of this study is to investigate the effects of the porosity on the buckling results of a simply supported rectangular plate composed of fiber-reinforced laminated composite materials. The Navier method is used in the solution of the problem. In the numerical results, the effects of the porosity coefficients and models, the fiber orientation angles and the sequence of laminas on the critical buckling loads are investigated.

2. Equations

In figure 1, a simply supported fiber-reinforced laminated plate with two layers under biaxial compressive loads (N_0) is shown with X_1, X_2, X_3 coordinate system. The height of laminas (h_l) is equal to each other.

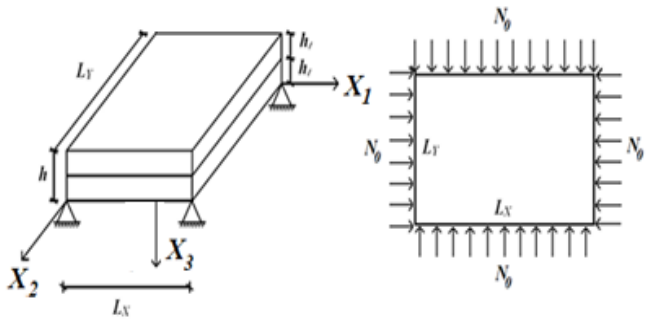

Figure 1. A simply supported fiber-reinforced laminated porous plate subjected to biaxial compressive loads.

According to the first shear deformation plate theory, the strain components are expressed in terms of displacement as follows;

$$\varepsilon_{X_1X_1} = \frac{\partial u_{01}}{\partial X_1} + X_3\frac{\partial \emptyset_{X_1}}{\partial X_1} \qquad \varepsilon_{X_2X_2} = \frac{\partial u_{02}}{\partial X_2} + X_3\frac{\partial \emptyset_{X_2}}{\partial X_2} \tag{1}$$

$$\gamma_{X_1X_2} = \frac{\partial u_{02}}{\partial X_2} + \frac{\partial u_{02}}{\partial X_1} + X_3\left(\frac{\partial \emptyset_{X_1}}{\partial X_2} + \frac{\partial \emptyset_{X_2}}{\partial X_1}\right) \tag{2}$$

$$\gamma_{X_1X_3} = \frac{\partial u_{03}}{\partial X_1} + \emptyset_{X_1}, \qquad \gamma_{X_2X_3} = \frac{\partial u_{03}}{\partial X_2} + \emptyset_{X_2}, \tag{3}$$

$$\varepsilon_{X_3X_3} = 0$$

where $\boldsymbol{u_{01}}$, $\boldsymbol{u_{02}}$ and $\boldsymbol{u_{03}}$ indicate displacements in $\boldsymbol{X_1}$, $\boldsymbol{X_2}$ and $\boldsymbol{X_3}$ directions, respectively. In the porosity distribution of each lamina, three different porosity distribution models are used. These porosity distribution models are shown in figure 2. In model 1, the voids spread uniformly in through the height. In model 2, the voids stack in the middle of laminas. In model 3, the voids spread the voids stack in the upper and lower surfaces of the laminas.

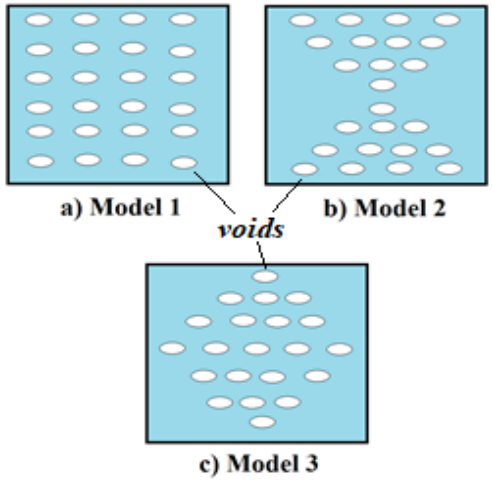

Figure 2. Porosity Distribution Models in Laminas. a) Model 1, b) Model 2 and c) Model 3.

According to these models, the effective material properties (P) such as Young Modulus, Poisson's ratio etc. are given as follows;

$$P(a) = P(1-a) \qquad \text{for model 1} \tag{4a}$$

$$P(a) = P\left(1 - a\frac{2\,|Y|}{h_l}\right) \qquad \text{for model 2} \tag{4b}$$

$$P(a) = P\left(1 - \frac{a}{2}\left(1 - \frac{2\,|Y|}{h_l}\right)\right) \qquad \text{for model 3} \tag{4c}$$

In equation 4, a (a<<1) indicates the volume fraction of porosity. Constitutive relations of orthotropic laminated plate for nth layer with porosity effect are given as follows:

$$\begin{Bmatrix}\sigma_{X_1X_1}\\ \sigma_{X_2X_2}\\ \sigma_{X_1X_2}\end{Bmatrix}^{(n)} = \begin{bmatrix}\overline{Q}_{11}(a) & \overline{Q}_{12}(a) & \overline{Q}_{16}(a)\\ \overline{Q}_{12}(a) & \overline{Q}_{22}(a) & \overline{Q}_{26}(a)\\ \overline{Q}_{16}(a) & \overline{Q}_{26}(a) & \overline{Q}_{66}(a)\end{bmatrix}^{(n)}$$

$$\begin{Bmatrix}\frac{\partial u_{01}}{\partial X_1} - X_3\frac{\partial^2 u_{03}}{\partial {X_1}^2}\\ \frac{\partial u_{02}}{\partial X_2} - X_3\frac{\partial^2 u_{03}}{\partial {X_2}^2}\\ \frac{\partial u_{01}}{\partial X_2} + \frac{\partial u_{02}}{\partial X_1} - X_3\frac{\partial^2 u_{03}}{\partial {X_2}^2} - X_3\frac{\partial^2 u_{03}}{\partial {X_1}^2}\end{Bmatrix}^{(n)} \tag{5a}$$

$$\begin{Bmatrix}\sigma_{X_2X_3}\\ \sigma_{X_1X_3}\end{Bmatrix}^{(n)} = \begin{bmatrix}\bar{Q}_{44}(a) & \bar{Q}_{45}(a)\\ \bar{Q}_{45}(a) & \bar{Q}_{55}(a)\end{bmatrix}^{(n)}\begin{Bmatrix}\frac{\partial u_{02}}{\partial X_2} - \frac{\partial u_{03}}{\partial X_2}\\ \frac{\partial u_{03}}{\partial X_1} - \frac{\partial u_{03}}{\partial X_1}\end{Bmatrix}^{(n)} \tag{5b}$$

where $\overline{\boldsymbol{Q}}_{ij}(a)$ indicates the components of stiffness tensor which depends the porosity parameter (a) are presented as follows:

$$\overline{Q}_{11}(a) = Q_{11}(a)cos^4\theta + 2(Q_{12}(a) + 2Q_{66}(a))sin^2\theta cos^2\theta + Q_{22}(a)sin^4\theta$$

$$\overline{Q}_{12}(a) = \left(Q_{11}(a) + Q_{22}(a) - 4Q_{66}(a)\right)sin^2\theta cos^2\theta + Q_{12}(a)(sin^4\theta + cos^4\theta)$$

$$\overline{Q}_{22}(a) = Q_{11}(a)sin^4\theta + 2\big(Q_{12}(a) + 2Q_{66}(a)\big) sin^2\theta cos^2\theta + Q_{22}(a)cos^4\theta$$

$$\overline{Q}_{16}(a) = \big(Q_{11}(a) - Q_{12}(a) - 2Q_{66}(a)\big)sin\theta cos^3\theta + (Q_{12}(a) - Q_{22}(a) + 2Q_{66}(a))sin^3\theta cos\theta$$

$$\overline{Q}_{26}(a) = \big(Q_{11}(a) - Q_{12}(a) - 2Q_{66}(a)\big)sin^3\theta cos\theta + (Q_{12}(a) - Q_{22}(a) + 2Q_{66}(a))sin\theta cos^3\theta$$

$$\bar{Q}_{44}(a) = Q_{44}(a)\cos^2\theta + Q_{55}(a)\sin^2\theta$$

$$\bar{Q}_{45}(a) = (Q_{55}(a) - Q_{44}(a))\cos\theta\sin\theta$$

$$\bar{Q}_{55}(a) = Q_{44}(a)\sin^2\theta + Q_{55}(a)\cos^2\theta \quad (6)$$

where, $\boldsymbol{\theta}$ is the fiber orientation angle. The components of the $\boldsymbol{Q_{ij}}$ are given as follows;

$$Q_{11}(a) = \frac{E_1(a)}{1 - \nu_{12}(a)\nu_{21}(a)}\ ,$$

$$Q_{22}(T) = \frac{E_2(a)}{1 - \nu_{12}(a)\nu_{21}(a)}$$

$$Q_{12}(a) = \frac{\nu_{12}E_2(a)}{1 - \nu_{12}(a)\nu_{21}(a)} = \frac{\nu_{21}E_1(a)}{1 - \nu_{12}(a)\nu_{21}(a)}$$

$$Q_{44}^{(n)}(a) = G_{23}^{(n)}(a) \qquad Q_{55}^{(n)}(a) = G_{13}^{(n)}(a)$$

$$Q_{21}(a) = \frac{\nu_{12}(a)E_2(a)}{1 - \nu_{12}(a)\nu_{21}(a)} = \frac{\nu_{21}E_1(a)}{1 - \nu_{12}(a)\nu_{21}(a)}$$

$$Q_{66}(a) = G_{12}(a) \quad (7)$$

Stress resultants are given as follows;

$$\begin{Bmatrix} N_{X_1X_1} \\ N_{X_2X_2} \\ N_{X_1X_2} \\ M_{X_1X_1} \\ M_{X_2X_2} \\ M_{X_1X_2} \end{Bmatrix} = \begin{bmatrix} \begin{bmatrix} A_{11} & A_{12} & A_{13} \\ A_{21} & A_{22} & A_{23} \\ A_{31} & A_{32} & A_{33} \end{bmatrix} & \begin{bmatrix} B_{11} & B_{12} & B_{13} \\ B_{21} & B_{22} & B_{23} \\ B_{31} & B_{32} & B_{33} \end{bmatrix} \\ \begin{bmatrix} B_{11} & B_{12} & B_{13} \\ B_{21} & B_{22} & B_{23} \\ B_{31} & B_{32} & B_{33} \end{bmatrix} & \begin{bmatrix} D_{11} & D_{12} & D_{13} \\ D_{21} & D_{22} & D_{23} \\ D_{31} & D_{32} & D_{33} \end{bmatrix} \end{bmatrix} \begin{Bmatrix} \frac{\partial u_{01}}{\partial X_1} \\ \frac{\partial u_{02}}{\partial X_2} \\ \frac{\partial u_{01}}{\partial X_2} + \frac{\partial u_{02}}{\partial X_1} \\ \frac{\partial \emptyset_{X_1}}{\partial X_1} \\ \frac{\partial \emptyset_{X_2}}{\partial X_2} \\ \frac{\partial \emptyset_{X_1}}{\partial X_2} + \frac{\partial \emptyset_{X_2}}{\partial X_1} \end{Bmatrix} \quad (8a)$$

$$\begin{Bmatrix} Q_{X_2} \\ Q_{X_1} \end{Bmatrix} = K \begin{bmatrix} A_{44} & A_{45} \\ A_{45} & A_{55} \end{bmatrix} \begin{bmatrix} \frac{\partial u_{03}}{\partial X_2} + \emptyset_{X_2} \\ \frac{\partial u_{03}}{\partial X_1} + \emptyset_{X_1} \end{bmatrix} \quad (8b)$$

Where $\boldsymbol{A_{ij}}$, $\boldsymbol{B_{ij}}$ and $\boldsymbol{D_{ij}}$ are extensional stiffness, bending – extensional coupling stiffness, and bending stiffness respectively, K indicates the shear correction coefficient;

$$A_{ij}(a) = \sum_{k=1}^{n} \overline{Q}_{ij}^{(n)}(a)(z_{n+1} - z_n) \quad (9a)$$

$$B_{ij}(a) = \frac{1}{2}\sum_{k=1}^{n} \overline{Q}_{ij}^{(n)}(a)(z_{n+1}^2 - z_n^2) \quad (9b)$$

$$D_{ij}(a) = \frac{1}{3}\sum_{k=1}^{n} \overline{Q}_{ij}^{(n)}(a)(z_{n+1}^3 - z_n^3) \quad (9c)$$

The governing equations of the problem are presented as follows;

$$\frac{\partial N_{X_1X_1}}{\partial X_1} + \frac{\partial N_{X_1X_2}}{\partial X_2} = 0 \quad (10a)$$

$$\frac{\partial N_{X_1X_2}}{\partial X_1} + \frac{\partial N_{X_2X_2}}{\partial X_2} = 0 \quad (10b)$$

$$\frac{\partial \mathrm{Q}_{\mathrm{X}_1}}{\partial \mathrm{X}_1} + \frac{\partial \mathrm{Q}_{\mathrm{X}_2}}{\partial \mathrm{X}_2} = 0 \quad (10c)$$

$$\frac{\partial M_{X_1X_1}}{\partial X_1} + \frac{\partial M_{X_1X_2}}{\partial X_2} - Q_{X_1} = 0 \quad (10d)$$

$$\frac{\partial M_{X_1X_2}}{\partial X_1} + \frac{\partial M_{X_2X_2}}{\partial X_2} - Q_{X_2} = 0 \quad (10e)$$

In the solution of the governing equations, the Navier method is used. The boundary conditions and displacement fields are presented as follows:

$$u_{01}(0, X_2) = 0, \quad u_{01}(a, X_2) = 0, \quad u_{02}(X_1, 0) = 0, \quad u_{02}(X_1, b) = 0, \quad (11a)$$

$$u_{03}(X_1, 0) = 0, \quad u_{03}(X_1, b) = 0, \quad u_{03}(0, X_2) = 0, \quad u_{03}(a, X_2) = 0, \quad (11b)$$

$$\emptyset_{X_1}(X_1, 0) = 0, \quad \emptyset_{X_1}(X_1, b) = 0, \quad \emptyset_{X_2}(0, X_2) = 0, \quad \emptyset_{X_2}(a, X_2) = 0, \quad (11c)$$

$$N_{X_1X_2}(0, X_2) = 0, \quad N_{X_1X_2}(a, X_2) = 0, \quad N_{X_1X_2}(X_1, 0) = 0, \quad N_{X_1X_2}(X_1, b) = 0 \quad (11d)$$

$$M_{X_1X_1}(0, X_2) = 0, \quad M_{X_1X_1}(a, X_2) = 0, \quad M_{X_2X_2}(X_1, 0) = 0, \quad M_{X_2X_2}(X_1, b) = 0 \quad (11e)$$

where $\boldsymbol{U_{1_{mn}}}$, $\boldsymbol{U_{2_{mn}}}$, $\boldsymbol{U_{3_{mn}}}$, $\boldsymbol{X_{X_{1_{mn}}}}$, $\boldsymbol{Y_{X_{2_{mn}}}}$ are displacement coefficients, $\boldsymbol{k = m\pi/L_{X_1}}$, $\boldsymbol{l = n\pi/L_{X_2}}$

Substituting eqs. (11-12) into eqs. (10) and then using Eigen-value procedure, the algebraic equation of the buckling problem is

given as follows;

$$\begin{bmatrix} p_{11} & p_{12} & 0 & p_{14} & p_{15} \\ p_{12} & p_{22} & 0 & p_{24} & p_{25} \\ 0 & 0 & p_{33}-N_0(k^2+sl^2) & p_{34} & p_{35} \\ p_{14} & p_{24} & p_{34} & p_{44} & p_{45} \\ p_{15} & p_{25} & p_{35} & p_{45} & p_{55} \end{bmatrix} \begin{Bmatrix} U_{1mn} \\ U_{2mn} \\ U_{3mn} \\ X_{X_1 mn} \\ Y_{X_2 mn} \end{Bmatrix} = \begin{Bmatrix} 0 \\ 0 \\ 0 \\ 0 \\ 0 \end{Bmatrix} \tag{13}$$

where,

$$\begin{aligned} p_{11} &= (A_{11}(a)k^2 + A_{66}(a)l^2), \\ p_{12} &= (A_{12}(a) + A_{66}(a))kl \\ p_{13} &= 0, \quad p_{14} = 2B_{16}(a)kl \\ p_{15} &= (B_{16}(a)k^2 + B_{26}(a)l^2), \\ p_{22} &= (A_{66}(a)k^2 + A_{22}(a)l^2), \quad p_{23} = 0, \\ p_{24} &= p_{15}, \quad p_{25} = B_{26}(a)kl, \\ p_{33} &= K(A_{55}(a)k^2 + A_{44}(a)l^2), \quad p_{34} = KA_{55}(a)k, \\ p_{35} &= KA_{44}(a)l, \\ p_{44} &= (D_{11}(a)k^2 + D_{22}(a)l^2 + KA_{55}(a)) \\ p_{45} &= \big(D_{12}(a) + D_{66}(a)\big)kl, \\ p_{55} &= (D_{66}(a)k^2 + D_{22}(a)l^2 + KA_{44}(a)) \\ \ddot{p}_{44} &= p_{44} - p_{14}\frac{c_1}{c_0} - p_{24}\frac{c_2}{c_0}, \\ \ddot{p}_{45} &= p_{45} - p_{15}\frac{c_1}{c_0} - p_{25}\frac{c_2}{c_0} \\ \ddot{p}_{55} &= p_{55} - p_{15}\frac{c_3}{c_0} - p_{25}\frac{c_4}{c_0}, \end{aligned} \tag{14}$$

$$c_0 = p_{11}p_{22} - p_{12}p_{12},$$

$$c_1 = p_{14}p_{22} - p_{12}p_{24}, \quad c_0 = p_{11}p_{24} - p_{12}p_{14},$$

$$c_3 = p_{15}p_{22} - p_{12}p_{25}, \quad c_4 = p_{11}p_{25} - p_{12}p_{15},$$

After the solution of the equation (13), the critical buckling load is expressed as follows;

$$N_{mn} = \frac{1}{k^2 + sl^2} \left(\frac{p_{34}\ddot{p}_{55} - p_{35}\ddot{p}_{45}}{\ddot{p}_{44}\ddot{p}_{55} - \ddot{p}_{45}\ddot{p}_{45}} p_{34} - \frac{\ddot{p}_{44}p_{35} - \ddot{p}_{45}p_{34}}{\ddot{p}_{44}\ddot{p}_{55} - \ddot{p}_{45}\ddot{p}_{45}} p_{35}\right) \tag{15}$$

Dimensionless fundamental frequency $\bar{\boldsymbol{N}}_{\boldsymbol{mn}}$ is defined as follows;

$$\bar{N}_{mn} = N_{mn}\left(\frac{{L_{X_1}}^2}{E_{02}h^3}\right) \tag{16}$$

3. Numerical Results

In the numerical examples, the effects of porosity coefficients, fiber orientation angles and different porosity models on the critical buckling loads of the porous fiber-reinforced laminated plate are investigated. In the numerical study, the material of the plate is considered as graphite-epoxy and its material parameters are; E_1=150 GPa, E_2=9 GPa, E_3=9 GPa, G_{12}=7,1 GPa, G_{23}=2,5 GPa, G_{13}=7,1 GPa, ν_{12}= ν_{21}=0.3. The geometry properties of the plate are selected as $\boldsymbol{L_{X_1}} = \mathbf{3m}$, $\boldsymbol{L_{X_2}} = \mathbf{3m}$, h=0.3 m.

In figures 3, 4 and 5, the relationship between the fiber orientation angle (θ) and dimensionless critical buckling load ($\boldsymbol{N_{mn}}$) is presented for different sequence of laminas, different porosity coefficients (a) and porosity distribution models for buckling mode 1-1 , mode 2-2 and mode 3-3, respectively. In these figures, *0/θ* and *θ/-θ* the sequence of laminas are used. It is seen from figures 3,4 and 5, the porosity distribution has a great influence on behavior of the fiber orientation angles and the buckling responses. In different porosity distribution models, the effects of the fiber orientation angles on the buckling responses differ considerably. Especially, in model 1, the buckling results are very sensitive to fiber orientation angles. This is because the voids uniformly spread through all volume of material. So, the rigidity of laminas in model 1 is lower than the other models. In addition, the effects of the porosity parameters on the buckling vary according to different porosity distribution models. With increasing in the number of buckling modes, the effects of the porosity on the buckling increase considerably.

In order to get more see the effects of the porosity coefficient, the relationship between the porosity parameters (a) and dimensionless critical buckling load ($\boldsymbol{N_{mn}}$) is plotted in figure 6 for different sequences of laminas, different porosity distribution models and fiber orientation angles for buckling mode 1-1. Figure 6 shows that the sequence of lamina very effective in the effects of the porosity on the bucking. The effects of porosity in *θ/-θ* sequence are bigger than those of *0/θ* sequence. The difference among the dimensionless critical buckling loads in *θ/-θ* sequence is bigger than *0/θ* sequence. In *θ/-θ* sequence, because the fiber direction does not coincide with the principal axes of laminas in all laminas, the rigidity of plate in *θ/-θ* is lower than *0/θ* sequence. So, the *θ/-θ* sequence is more sensitive with porosity effects in contrast with *0/θ* sequence. Also, it is more clearly seen from figure 6 that the critical buckling loads decrease with increasing porosity parameter *a* because the strength of plates naturally decreases with increasing porosity.

4. Conclusions

In this paper, the effects of porosity and its distribution models on the buckling behavior of a laminated plate are investigated. Three porosity distribution models are used. The governing equations of the considered problem are solved by using Navier method for a simply supported laminated porous plate. In the numerical results, the dimensionless critical buckling loads are obtained with different porosity coefficients, fiber orientation angles, the sequence of laminas, and porosity models. In obtaining from numerical results, the porosity changes the buckling behavior of laminated plates, significantly. The porosity distribution and the sequence of laminas have a great influence on the buckling behavior of fiber-reinforced laminated plates. The critical buckling loads decrease with increasing porosity parameters. In the different sequence of laminas, the buckling responses of the laminated plate differ with porosity, considerably. With suitable choosing the sequence of laminas, the effects of the porosity can be decreased to a certain level.

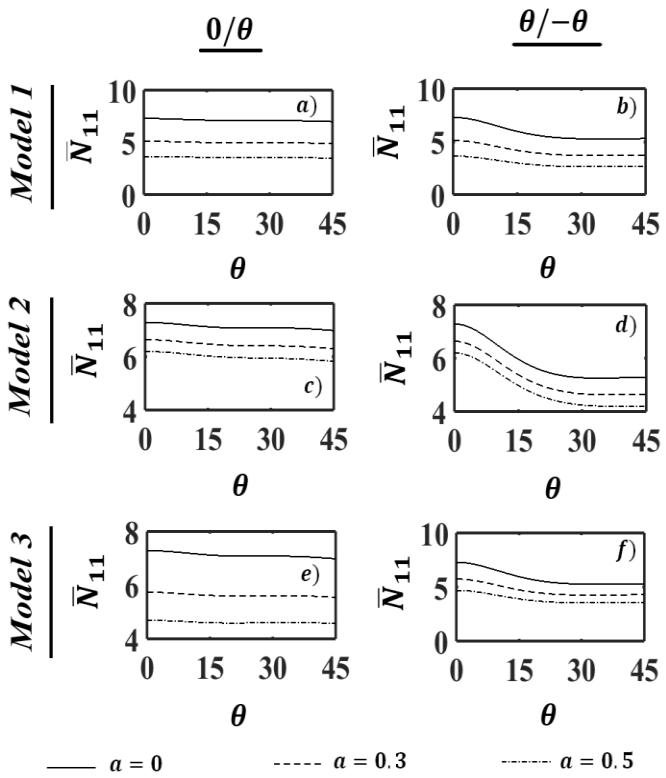

Figure 3. The relationship between the fiber orientation angle (θ) and dimensionless critical buckling load ($\bar{N}_{mn}$) for a different sequences of laminas, different porosity distribution model and parameters for buckling mode 1-1.

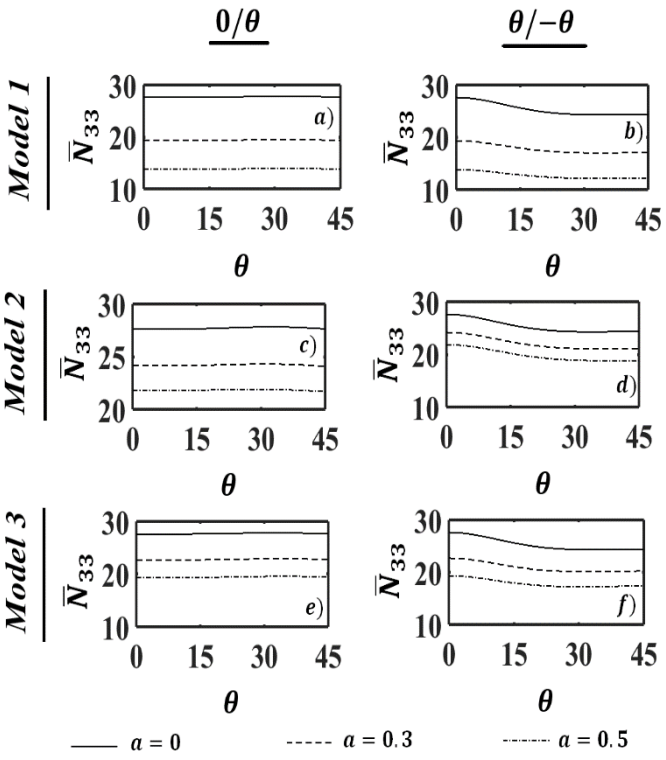

Figure 5. The relationship between the fiber orientation angle (θ) and dimensionless critical buckling load ($\bar{N}_{mn}$) for different porosity distribution model and parameters for buckling mode 3-3.

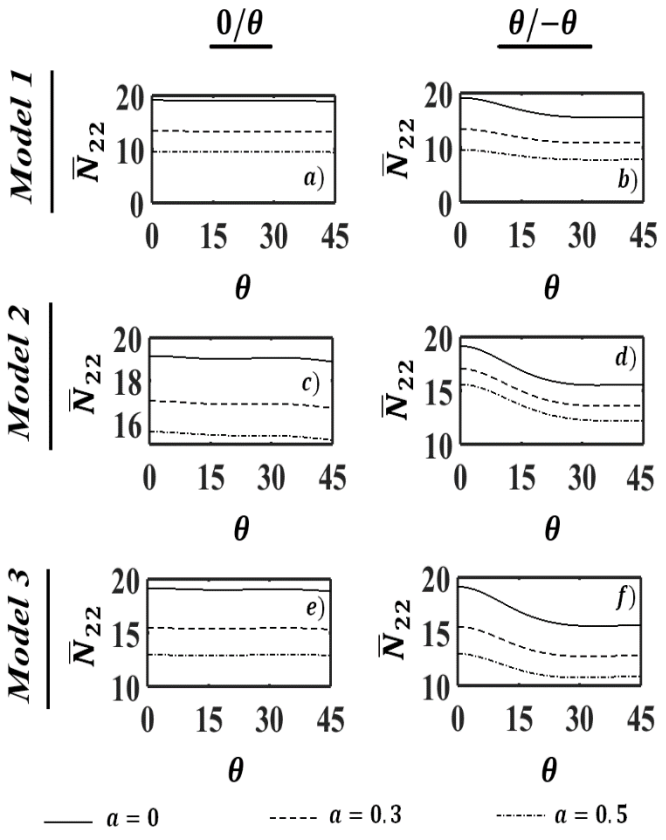

Figure 4. The relationship between the fiber orientation angle (θ) and dimensionless critical buckling load ($\bar{N}_{mn}$) for a different porosity distribution model and parameters for buckling mode 2-2.

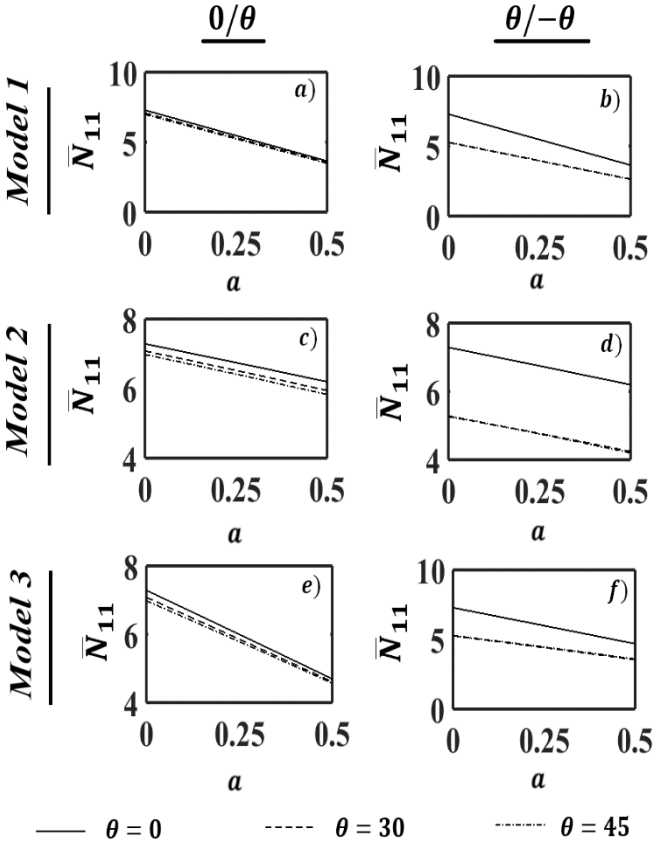

Figure 6. The relationship between the porosity coefficient (a) and dimensionless critical buckling load ($\bar{N}_{mn}$) for different porosity distribution model and fiber orientation angles for buckling mode 1-1.

References

[1] Rezaei A.S., Saidi A.R., 2015, Exact solution for free vibration of thick rectangular plates made of porous materials, Composite Structures 134: 1051–1060.

[2] Akbaş Ş.D., 2017, Vibration and static analysis of functionally graded porous plates, Journal of Applied and Computational Mechanics 3(3): 199–207.

[3] Rezaei A.S., Saidi A.R., Abrishamdari M., Mohammadi M.H.P., 2017, Natural frequencies of functionally graded plates with porosities via a simple four variable plate theory: An analytical approach, Thin-Walled Structures 120: 366–377.

[4] Wang Y.Q., Zu J.W., 2017, Vibration behaviors of functionally graded rectangular plates with porosities and moving in thermal environment, Aerospace Science and Technology 69: 550–562.

[5] Askari M., Saidi A.R., Rezaei A.S., 2017, On natural frequencies of Levy-type thick porous-cellular plates surrounded by piezoelectric layers, Composite Structures 179: 340–354.

[6] Ebrahimi F., Jafari A., Barati M.R., 2017, Vibration analysis of magneto-electro-elastic heterogeneous porous material plates resting on elastic foundations, Thin-Walled Structures 119: 33–46.

[7] Zhao J., Choe K., Xie F., Wang A., Shuai C., Wang Q., 2018, Three-dimensional exact solution for vibration analysis of thick functionally graded porous (FGP) rectangular plates with arbitrary boundary conditions, Composites Part B: Engineering 155: 369–381.

[8] Yang J., Chen D., Kitipornchai S., 2018, Buckling and free vibration analyses of functionally graded graphene reinforced porous nanocomposite plates based on Chebyshev-Ritz method, Composite Structures 193: 281–294.

[9] Arshid E., Khorshidvand A.R., 2018, Free vibration analysis of saturated porous FG circular plates integrated with piezoelectric actuators via differential quadrature method, Thin-Walled Structures 125: 220–233.

[10] Gao K., Gao W., Chen D., Yang J., 2018, Nonlinear free vibration of functionally graded graphene platelets reinforced porous nanocomposite plates resting on elastic foundation, Composite Structures 204: 831–846.

[11] Zhao J., Xie F., Wang A., Shuai C., Tang J., Wang Q., 2019, A unified solution for the vibration analysis of functionally graded porous (FGP) shallow shells with general boundary conditions, Composites Part B: Engineering 156: 406–424.

[12] Demirhan P.A., Taskin V., 2019, Bending and free vibration analysis of Levy-type porous functionally graded plate using state space approach, Composites Part B: Engineering 160: 661–676.

[13] Kim J., Żur K.K., Reddy J.N., 2019, Bending, free vibration, and buckling of modified couples stress-based functionally graded porous micro-plates, Composite Structures 209: 879–888.

[14] Heshmati M., Jalali S.K., 2019, Effect of radially graded porosity on the free vibration behavior of circular and annular sandwich plates, European Journal of Mechanics, A/Solids 74: 417–430.

[15] Xue Y., Jin G., Ma X., Chen H., Ye T., Chen M., Zhang Y., 2019, Free vibration analysis of porous plates with porosity distributions in the thickness and in-plane directions using isogeometric approach, International Journal of Mechanical Sciences 152: 346–362.

[16] Zhao J., Wang Q., Deng X., Choe K., Zhong R., Shuai C., 2019, Free vibrations of functionally graded porous rectangular plate with uniform elastic boundary conditions, Composites Part B: Engineering 168: 106–120.

[17] Karimiasl M., Ebrahimi F., Mahesh V., 2019, Nonlinear forced vibration of smart multiscale sandwich composite doubly curved porous shell, Thin-Walled Structures 143: 106-152.

[18] Huang X., Dong L., Wei G., Zhong D., 2019, Nonlinear free and forced vibrations of porous sigmoid functionally graded plates on nonlinear elastic foundations, Composite Structures 228: 1-11.

[19] Zhou K., Lin Z., Huang X., Hua H., 2019, Vibration and sound radiation analysis of temperature-dependent porous functionally graded material plates with general boundary conditions, Applied Acoustics 154: 236–250.

[20] Yüksel Y.Z., Akbaş Ş.D., 2018, Free vibration analysis of a cross-ply laminated plate in thermal environment, International Journal of Engineering and Applied Sciences 10(3): 176-189.

[21] Akbaş Ş.D., 2018, Forced vibration analysis of functionally graded porous deep beams, Composite Structures 186: 293-302.

[22] Akbaş Ş.D., 2018, Geometrically nonlinear analysis of functionally graded porous beams, Wind and Structures 27(1): 59-70.

[23] Akbaş Ş.D., 2017, Thermal effects on the vibration of functionally graded deep beams with porosity, International Journal of Applied Mechanics 9(05): 1750076.

[24] Akbaş Ş.D., 2017, Post-buckling responses of functionally graded beams with porosities, Steel and Composite Structures 24(5): 579-589.

[25] Akbaş Ş.D., 2017, Stability of a non-homogenous porous plate by using generalized differantial quadrature method, International Journal of Engineering and Applied Sciences 9: 147-155.

[26] Li Q., Wu D., Chen X., Liu L., Yu Y., Gao W., 2018, Nonlinear vibration and dynamic buckling analyses of sandwich functionally graded porous plate with graphene platelet reinforcement resting on Winkler–Pasternak elastic foundation, International Journal of Mechanical Sciences 148: 596-610.

[27] Nam V.H., Trung N.T., 2019, Buckling and postbuckling of porous cylindrical shells with functionally graded composite coating under torsion in thermal environment, Thin-Walled Structures 144: 1-14.

[28] Chen D., Yang J., Kitipornchai, S., 2019, Buckling and bending analyses of a novel functionally graded porous plate using Chebyshev-Ritz method, Archives of Civil and Mechanical Engineering 19(1): 157-170.

[29] Safaei B., Moradi-Dastjerdi R., Behdinan K., Chu F., 2019, Critical buckling temperature and force in porous sandwich plates with CNT-reinforced nanocomposite layers, Aerospace Science and Technology 91: 175-185.

[30] Jabbari M., Joubaneh E.F., Mojahedin A., 2014, Thermal buckling analysis of porous circular plate with piezoelectric actuators based on first order shear deformation theory, International Journal of Mechanical Sciences 83: 57-64.

[31] Cong P.H., Chien T.M., Khoa N.D., Duc N.D., 2018, Nonlinear thermomechanical buckling and post-buckling response of porous FGM plates using Reddy's HSDT, Aerospace Science and Technology 77: 419-428.

[32] Dong Y.H., He L.W., Wang L., Li Y.H., Yang J., 2018, Buckling of spinning functionally graded graphene reinforced porous nanocomposite cylindrical shells: an analytical study, Aerospace Science and Technology 82: 466-478.

[33] Jabbari M., Joubaneh E.F., Khorshidvand A.R., Eslami M.R., 2013, Buckling analysis of porous circular plate with piezoelectric actuator layers under uniform radial compression, International Journal of Mechanical Sciences 70: 50-56.